THREE-DIMENSIONAL MIXED CONVECTION HEAT TRANSFER IN A PARTIALLY HEATED VENTILATED CAVITY

by

Hicham DOGHMI [*]***, Btissam ABOURIDA, Lahoucin BELARCHE, Mohamed SANNAD, and Meriem OUZAOUIT***

National School of Applied Sciences, Ibn Zohr University, Agadir, Morocco

Original scientific paper
https://doi.org/10.2298/TSCI180410193D

The 3-D mixed convective heat transfer inside a ventilated cavity partially heated is studied numerically by using control volume method. The heating square portion similar to the integrated electronic devices is placed on the left vertical wall of the enclosure. The right vertical wall is maintained at ambient temperature and all other walls are adiabatic.

The results are presented in terms of flow structures, temperature distribution, and global average Nusselt number for various combinations of thermal controlling parameters, namely, the Richardson number ($0 \leq Ri \leq 10$), the Reynolds number ($10 \leq Ri \leq 200$), the heating section dimension ($0. \leq \varepsilon \leq 0.7$), and the relative height of the openings $B = h/L = 1/8$. It is found that for the low Reynolds number the heat transfer process is carried out only by conduction. On the other hand, the highest thermal performance is achieved by reducing the heating section dimension.

Key words: *mixed convection, ventilated cavity, heat transfer, heating surface, 3-D, numerical simulation*

Introduction

Thermal dissipation of electronic components is one of the most common problems encountered in many engineering applications. In fact, the mixed convection processing 3-D ventilated cavities represents a simple and low-cost mode of cooling operation to ensure an optimal evacuation of the heat surplus and to control and optimize the cooling of the system. In addition, this phenomenon is also involved in many various engineering systems, such as the design of solar collectors, industrial processing, the thermal design of buildings, air conditioning, and others. This practical interest explains the existence of various studies. Hence, numerical and experimental studies of the 2-D laminar mixed convection in ventilated cavities have been reported by many authors [1-12] and their principal results showed that the interaction between the natural convection and the external forced convection plays a simultaneous role in the heat removal.

In references [13-22] the authors studied numerically the heat transfer process in ventilated air-cooled cavities for different inlet-outlet opening positions. They found that the increase of the thermal parameters (grand Reynolds number) and the optimal choice of the ventilation orientations can lead to the best cooling effectiveness. Rahman *et al.* [23] performed a numerical investigation of the effects of Reynolds and Prandtl numbers on mixed convection

* Corresponding author, e-mail: hicham.gte@gmail.com

inside a bi-dimensional square cavity containing a heated block. They indicated that the heat transfer rate increases with the increase of all the thermal parameters (Re, Pr, Ri) for different locations of the solid block.

Natural convection within 3-D enclosures with partially heated wall have been studied numerically by varying the thermal boundary conditions in [24, 25]. The principal results showed that the transition from conduction to convection regime ends at $\mathrm{Ra} = 10^5$ which result in a highly 3-D flow, with high lateral velocity components.

Stiriba *et al.* [26] investigated numerically the 3-D mixed convection inside an open cavity. Their results showed that the flow motion becomes unsteady with Kelvin-Helmholtz instabilities at the shear layer and the heat transfer rate increases significantly for $\mathrm{Re} = 10^3$ and $\mathrm{Gr} = 10^7$.

Moraga and Lopez [27] compared numerically the 3-D and 2-D mixed convection phenomenon inside an air-cooled cavity. They observed a major difference between the global Nusselt numbers calculated from the 2-D and the 3-D models. The 3-D model allowed the visualization of the flow structure for $\mathrm{Ri} = 10$ when $10 \leq \mathrm{Re} \leq 250$, and the estimation of the heat transfer rate for $\mathrm{Ri} < 1$ when $\mathrm{Re} = 500$.

Tariq *et al.* [28] studied numerically the mixed convection boundary-layer flow of a viscoelastic fluid due to horizontal elliptic cylinder with constant heat flux. Their principal results showed that the values of skin friction and Nusselt number rise with increase in mixed convection parameter.

A recent 3-D numerical investigation of the inlet opening effect on the mixed convection inside a 3-D ventilated cavity was presented by Doghmi *et al.* [29]. They concluded that the global average Nusselt number at the active walls increases with increasing Richardson numbers and the heat transfer rate increase and decrease at the hot and the cold wall respectively by increasing the inlet opening cross-section.

The previous works showed that 3-D approach gives a better idea of the flow structures and temperature distribution inside the cavity and leads to important results, compared to the 2-D approach. In fact, the literature review showed that very few studies considered mixed convection in 3-D ventilated cavities with a partially heated wall. This explains the choice of our present physical model, which intended to investigate numerically the effects of the thermal and geometrical parameters on the thermal transport and fluid-flow phenomena in this kind of enclosures.

Physical problem and governing equations

The configuration under study and coordinate system are presented in fig. 1. It consists of a 3-D ventilated cavity ($H = L$) which has an inlet opening with a rectangular cross-section of relative height $B = h/H$ located on the bottom of the left vertical wall, allowing the air flow to get in at a uniform velocity, u_{in}, and ambient temperature, T_{c}. Whereas the flow leaves via the outlet opening which has the same relative height $B = h/L$ as the entrance one. This opening is placed at the top of the opposite vertical wall. The isothermal, T_{h}, hot portion $\varepsilon = c/L$ is located at the middle of the left vertical, while the rest of the wall is adiabatic. The right vertical wall of the cavity is kept at the same temperature T_{c} as the external air-flow. The other four walls of the cavity are maintained adiabatic. A channel with the same cross-section and a length of ($L = 1$) is placed at the opening of the right vertical wall to extend the cavity and makes it possible to use the developed boundary conditions for the fluid-flow and heat transfer at the outlet.

The cooling fluid is considered laminar, Newtonian and incompressible with negligible viscous dissipation. All the thermophysical properties of the fluid are assumed constant except the density, giving rise to the buoyancy forces verifying the Boussinesq approximation.

The governing equations for the 3-D laminar incompressible fluid are expressed in the following dimensionless form:

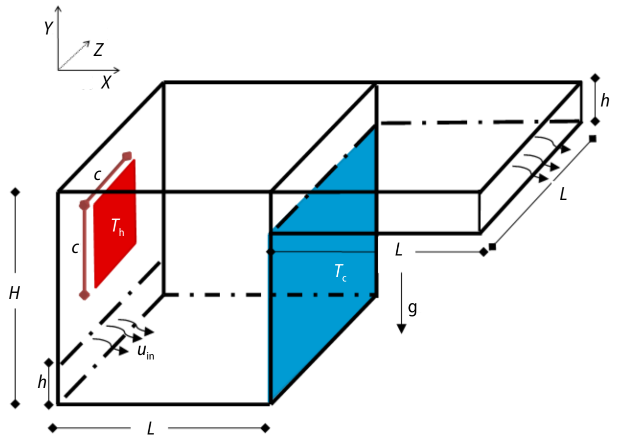

Figure 1. Studied configuration and co-ordinates

– Continuity equation:

$$\frac{\partial U}{\partial X}+\frac{\partial V}{\partial Y}+\frac{\partial W}{\partial Z}=0 \tag{1}$$

– Momentum equation in the *X*-direction:

$$U\frac{\partial U}{\partial X}+V\frac{\partial U}{\partial Y}+W\frac{\partial U}{\partial Z}=-\frac{\partial P}{\partial X}+\frac{1}{\mathrm{Re}}\left(\frac{\partial^2 U}{\partial X^2}+\frac{\partial^2 U}{\partial Y^2}+\frac{\partial^2 U}{\partial Z^2}\right) \tag{2}$$

– Momentum equation in the *Y*-direction:

$$U\frac{\partial V}{\partial X}+V\frac{\partial V}{\partial Y}+W\frac{\partial V}{\partial Z}=-\frac{\partial P}{\partial Y}+\frac{1}{\mathrm{Re}}\left(\frac{\partial^2 V}{\partial X^2}+\frac{\partial^2 V}{\partial Y^2}+\frac{\partial^2 V}{\partial Z^2}\right)+\frac{\mathrm{Gr}}{\mathrm{Re}^2}\theta \tag{3}$$

– Momentum equation in the *Z*-direction:

$$U\frac{\partial W}{\partial X}+V\frac{\partial W}{\partial Y}+W\frac{\partial W}{\partial Z}=-\frac{\partial P}{\partial Z}+\frac{1}{\mathrm{Re}}\left(\frac{\partial^2 W}{\partial X^2}+\frac{\partial^2 W}{\partial Y^2}+\frac{\partial^2 W}{\partial Z^2}\right) \tag{4}$$

– Energy equation:

$$U\frac{\partial \theta}{\partial X}+V\frac{\partial \theta}{\partial Y}+W\frac{\partial \theta}{\partial Z}=\frac{1}{\mathrm{RePr}}\left(\frac{\partial^2 \theta}{\partial X^2}+\frac{\partial^2 \theta}{\partial Y^2}+\frac{\partial^2 \theta}{\partial Z^2}\right) \tag{5}$$

The non-dimensional variables are defined as:

$$X=\frac{x}{L},\quad Y=\frac{y}{L},\quad Z=\frac{z}{L} \tag{6}$$

$$U=\frac{u}{u_{\mathrm{in}}},\quad V=\frac{v}{u_{\mathrm{in}}},\quad W=\frac{w}{u_{\mathrm{in}}},\quad P=\frac{p-p_0}{\rho_0 u_{\mathrm{in}}^2},\quad \theta=\frac{T-T_c}{T_h-T_c} \tag{7}$$

where p_0 and ρ_0 are, respectively, the reference pressure and density, T_{h} – the temperature of the heated surface, T_{c} – the temperature of the cooled surface, p – the pressure, and U, V, and W, are the velocity components.

In the previous equations, the parameters Re, Gr, Ri, and Pr denote Reynold, Grashof, Richardson, and Prandtl numbers, respectively. These parameters are defined:

$$\mathrm{Re}=\frac{Lu_i}{\nu},\quad \mathrm{Gr}=\frac{g\beta L^3\left(T_h-T_c\right)}{\nu^2},\quad \mathrm{Ri}=\frac{\mathrm{Gr}}{\mathrm{Re}^2},\quad \mathrm{Pr}=\frac{\nu}{\alpha} \tag{8}$$

where β, ν, and α are the thermal expansion coefficient, the kinematic viscosity, and the thermal diffusivity, respectively.

The boundary conditions, associated to the problem are:

- $U=V=W=0$ on the rigid walls of the enclosure,
- $U=1$, $V=W=0$, $\theta_c=0$ at the inlet,
- $\theta_h=1$ on the heated section, $\partial\theta/\partial n=0$, elsewhere on the wall,
- $\theta_c=0$ on the right vertical cold wall,
- $\partial\theta/\partial n=0$, on other vertical and horizontal walls (n is the normal direction to the considered wall), and
- $\partial U/\partial X=0,\quad \partial\theta/\partial X=0,\quad V=W=0$ at the outlet.

The local Nusselt and the global average Nusselt numbers, characterizing the heat transfer on the heated walls are, respectively, defined by:

$$\mathrm{Nu}_{\mathrm{local}}\left(Y,Z\right)=\frac{\partial\theta}{\partial X}\quad \text{at}\quad X=0 \tag{9}$$

$$\mathrm{Nu}_h=\frac{1}{\varepsilon^2}\int_{\frac{1-\varepsilon}{2}}^{\frac{1+\varepsilon}{2}}\int \mathrm{Nu}_{\mathrm{local}}\left(Y,Z\right)\mathrm{d}Y\mathrm{d}Z \tag{10}$$

Numerical method

The continuity, energy and momentum equations of were solved by the home-developed FORTRAN code based on the finite volume's method developed by Patankar [30]. The SIMPLEC algorithm is used to couple the momentum conservation and continuity equations. A combination between the Gauss-Seidel method and the tridiagonal matrix algorithm (TDMA) also known as Thomas's algorithm is realized to solve iteratively the algebraic equations system. The convergence of solutions is established according to the following criterion:

$$\sum_{i,j,k=1}^{i\max,\,j\max,\,k\max}\frac{\left|\phi_{i,j,k}^{m+1}-\phi_{i,j,k}^{m}\right|}{\left|\phi_{i,j,k}^{m+1}\right|}\le 10^{-5} \tag{11}$$

where ϕ represents a dependent variable U, V, W, T, and P, the indices i, j, and k indicate the grid positions, n represents the iteration number.

Preliminary tests were used to check the grid independent of the solution using different uniform grid sizes. The grid $91\times 71\times 71$ was estimated to be appropriate for the present study since it permits a good compromise between the computational cost and the accuracy of the obtained results. In addition, the maximum deviation remains within 1.5% compared to further refined mesh to $101\times 91\times 91$.

The present computational model was checked in the case of natural convection heat transfer with the results presented by Frederick and Quiroz [24] and Ben-Cheikh *et al.* [25] with a heating section of dimension e = 0.5 placed on the vertical wall of the cavity, tab. 1. In addition, the code was validated in the case of mixed convection in a ventilated cavity with the existing 2-D and 3-D studies of Moraga and Lopez [27] in terms of isotherms shown in fig 2.

Table 1. Comparison of the numerical code with published results in terms U_{max} and V_{max} for $Z = 0.5$ and Ra = 10^5

[24]		[25]		Present study	
U_{max}	V_{max}	U_{max}	V_{max}	U_{max}	V_{max}
35.9146	63.2177	35.9436	65.6693	36.402	64.7033

It can be seen from this comparison that there is a good agreement between the present results and those presented by the mentioned references.

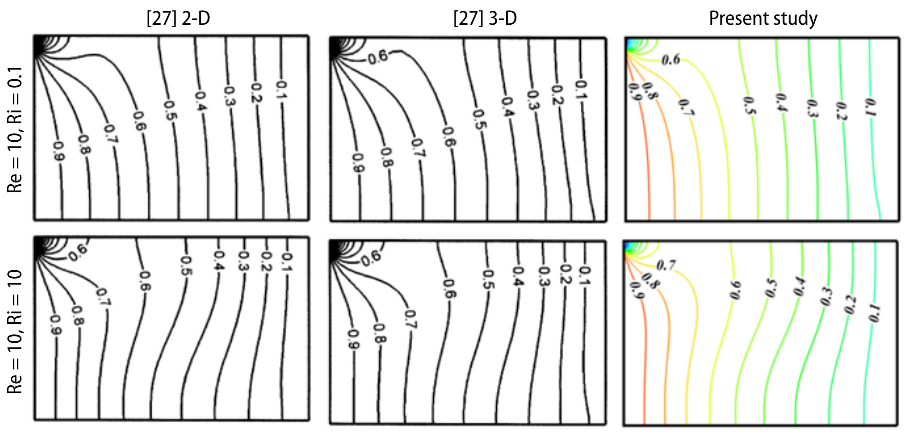

Figure 2. Comparison between the isotherm-lines obtained at the middle plane $Z = 0.5$ and those presented by Moraga and Lopez [27]

Results and discussion

Numerical computations are performed with an aim to examine the effect of thermal and geometrical parameters on the thermal transfer and fluid-flow phenomena within the 3-D ventilated cavity. The computed thermal and flow fields are analyzed in terms of streamlines, temperature distribution, the velocity components and average Nusselt number over a wide range of Reynolds number ($10 \leq \text{Re} \leq 200$), Richardson number ($0 \leq \text{Ri} \leq 10$), and the heating surface dimension $0.3 \leq \varepsilon \leq 0.7$. The Prandtl number is that of air $\text{Pr} = 0.72$, while the relative height of the inlet-outlet openings B is fixed to 1/8.

Effect of the thermal parameters

The analysis of the isotherms and streamlines in different planes $(0 \leq Z \leq 1)$ are depicted in fig. 3 which indicate a good symmetry with respect to the plane $Z = 0.5$. This is due to the geometrical symmetry and adopted thermal boundary conditions. Based on different preliminary tests the $Z = 0.5$, $Y = 0.5$, and $X = 0.025$ planes are found to be characterized by higher activity and seems to be adequate for the visualization of the dynamical and thermal fields inside the cavity.

To highlight the effect of the Reynolds and Richardson numbers on 3-D flow structure and the temperature distribution within the cavity for a constant value of the heating surface dimension $\varepsilon = 0.5$, hydrodynamic and thermal fields are shown in figs. 4-6.

The results indicate the existence of three modes of heat transfer regimes, depending on the governing parameter Richardson number values, which characterizes the relative importance of the buoyancy compared to the inertia forces. The first case is shown in fig. 4 for $\text{Ri} = 0$ and low

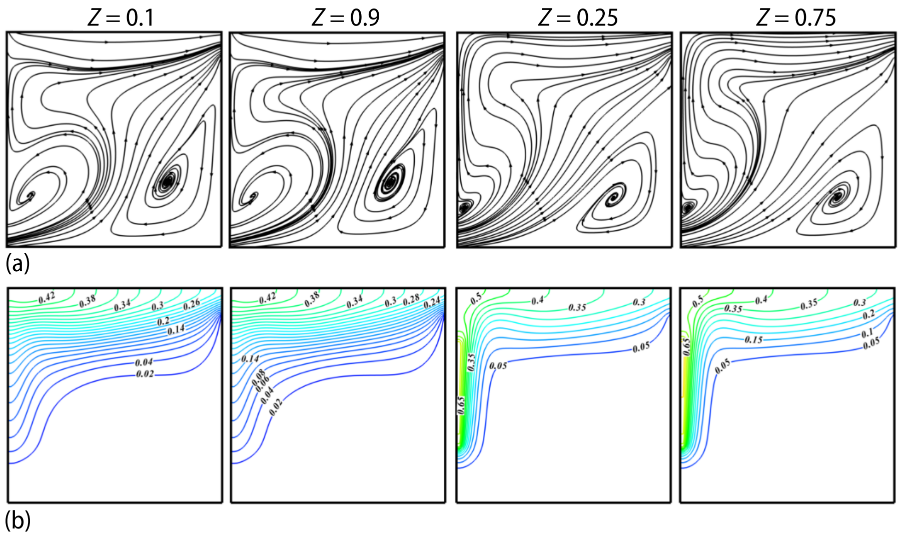

Figure 3. Streamlines (a) isotherm lines (b) at different *Z* planes for Re = 200 and Ri = 10

Reynolds numbers (Re = 10), the incoming fluid-flow is driven so slowly that the open lines preserve the same shape and occupy almost the whole cavity. They also show a perfect symmetry

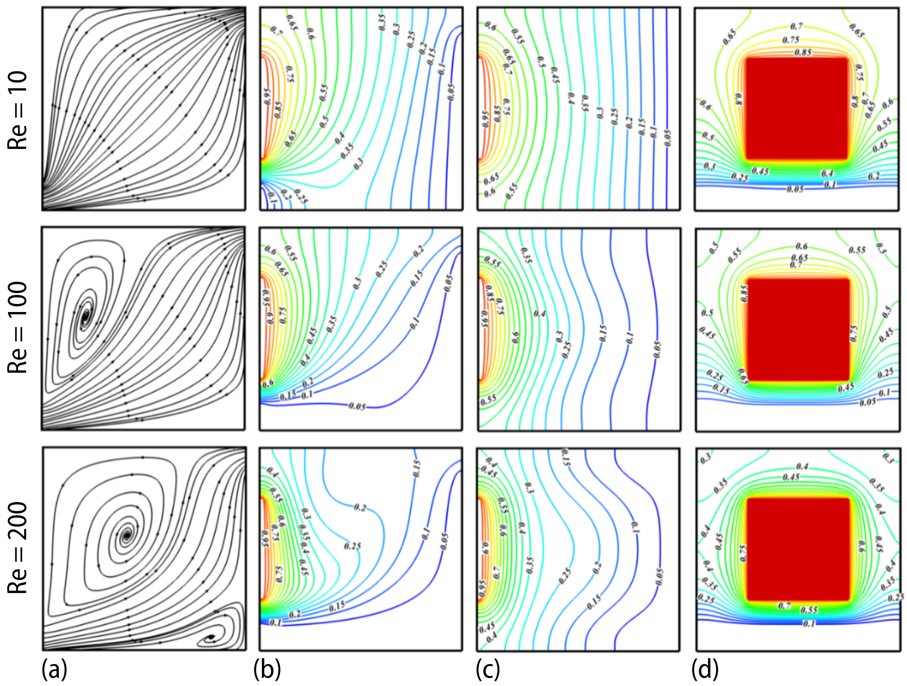

Figure 4. Streamlines (a) at the middle plane $Z = 0.5$ and isotherms in the vicinity of the heated surface at the planes, (b) $Z = 0.5$, (c) $Y = 0.5$, and (d) $X = 0.025$ for different values of Reynolds number when Ri = 0

with respect to the line joining the inlet and the outlet openings. The isotherms structure indicates that the high temperature region is uniformly concentrated and stratified at the vicinity of the heating surface, while the isotherms lines corresponding to lower and the medium temperature are parallel to each other in the remaining parts of the cavity, which signifies a thermal conduction heat transfer. The increase of the Reynolds number to moderate value ($\mathrm{Re} = 100$) leads to the formation of anti-clockwise vortex above the open lines of the accelerated forced flow. Furthermore, the size and the intensity of the upper vortex increases by increasing Reynolds number to 200 , while a small clockwise vortex appears at the right lower corner of the vertical cold wall. The distribution of the temperature inside the cavity shows that the lower values are related to the isotherms, which are oriented towards the outlet. However, a distortion of the temperature isolines in the core of the cavity is observed which, means that the inertia forces are playing the main role in the flow transport.

As the Richardson number increases to Ri = 1, fig. 5, and for low Reynolds number ($\mathrm{Re} = 10$), the streamlines and the isotherms lines have similar behavior with small difference compared to the previous case (Ri = 0). In fact, the interaction between the incoming flow and the heated surface is still weak to allow the variation of the fluid density and give rise to the particles movement. Furthermore, the flow structure is characterized by a small circulating cell above the inlet opening and the streamlines become distorted near the right vertical wall with the increase of the inertia forces. The isotherms are progressively tightened around the heated surface and are almost vertically inclined in the remaining part of the cavity. This is due to thermal interaction between the buoyancy effect provided from the heated surface and the incoming cold flow, which allows the installation of mixed convection.

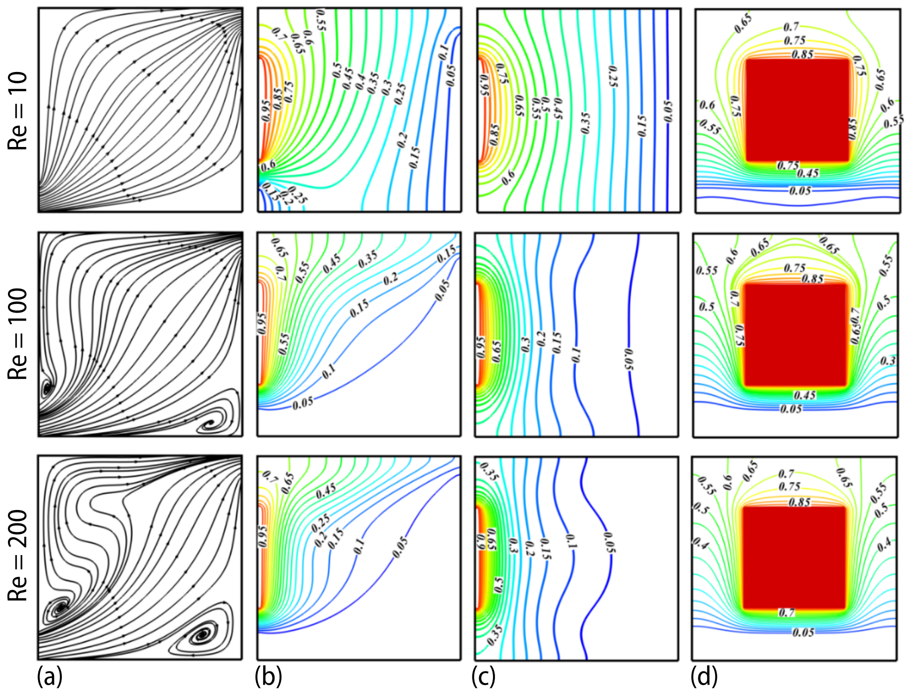

Figure 5. Streamlines (a) at the middle plane $Z = 0.5$ and isotherms at the planes, (b) $Z = 0.5$, (c) $Y = 0.5$, and (d) $X = 0.025$ for different values of Reynolds number when Ri = 1

At a higher value of the Richardson number (Ri = 10), fig. 6. The role of the natural convection in the cavity becomes more significant and consequently. The open lines related to the externally forced flow are affected by the heated surface and form convective circulating cell rotating in the clockwise direction near the cold wall. Thus, cell increases in size and intensity by increasing the Reynolds numbers. In fact, the boundary-layers become thinner at the vicinity of the heated surface and a part of the internal heated air interact favorably with the incoming cold flow and the cold wall since the buoyancy effects become the dominant mode of the mixed convection transport. For small Reynolds number (Re = 10), the temperature lines are uniformly distributed which indicate a lower heat transfer. As Reynolds number increases, the isotherms become vertically tightened near the heated surface and submit a slight deflection on the upper part of the cavity until the outlet, testifying of a noticeable increase in the convective heat exchange. On the other hand, the lower part of the cavity is at a uniform cold temperature, creating a thermally inactive zone, which increases in size when the flow motions become intense.

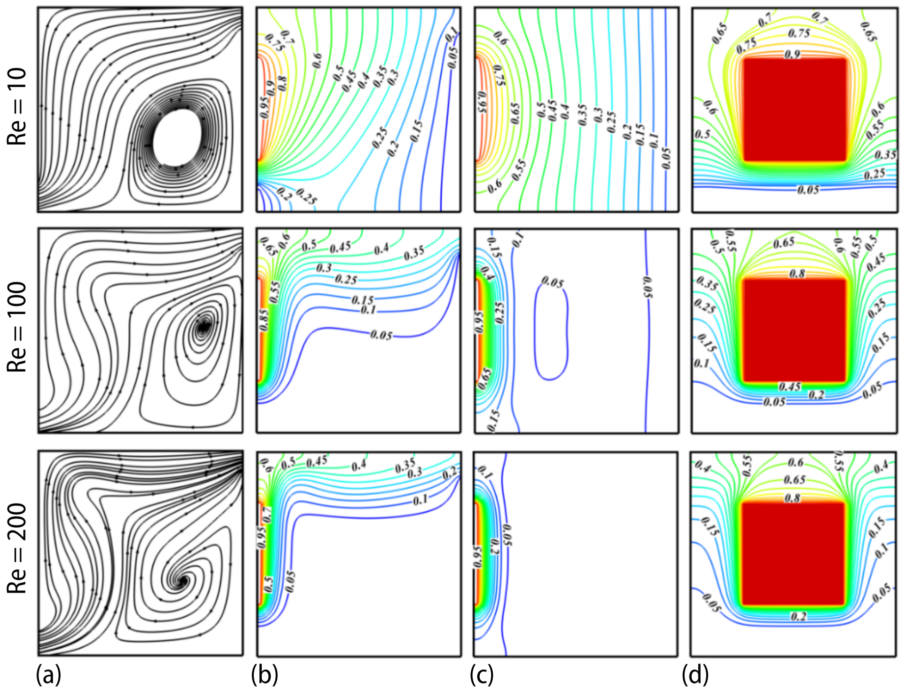

Figure 6. Streamlines (a) at the middle plane *Z* = 0.5 and isotherms at the planes, (b) *Z* = 0.5, (c) *Y* = 0.5, and (d) *X* = 0.025 for different values of Reynolds number when Ri = 10

Effect of heating section dimension

The impact of the heating section dimension on the flow motion, heat transfer and velocity profiles for $\mathrm{Ri} = 1$ and $\mathrm{Re} = 100$, are shown in figs. 7-9. For all the considered cases, the flow consists mainly of open lines directed to the outlet with two small re-circulation structures: the first cell is counter-clockwise rotating above the inlet opening and the other one is clockwise circulation and located in the vicinity of the left lower corner of the cavity. By in-

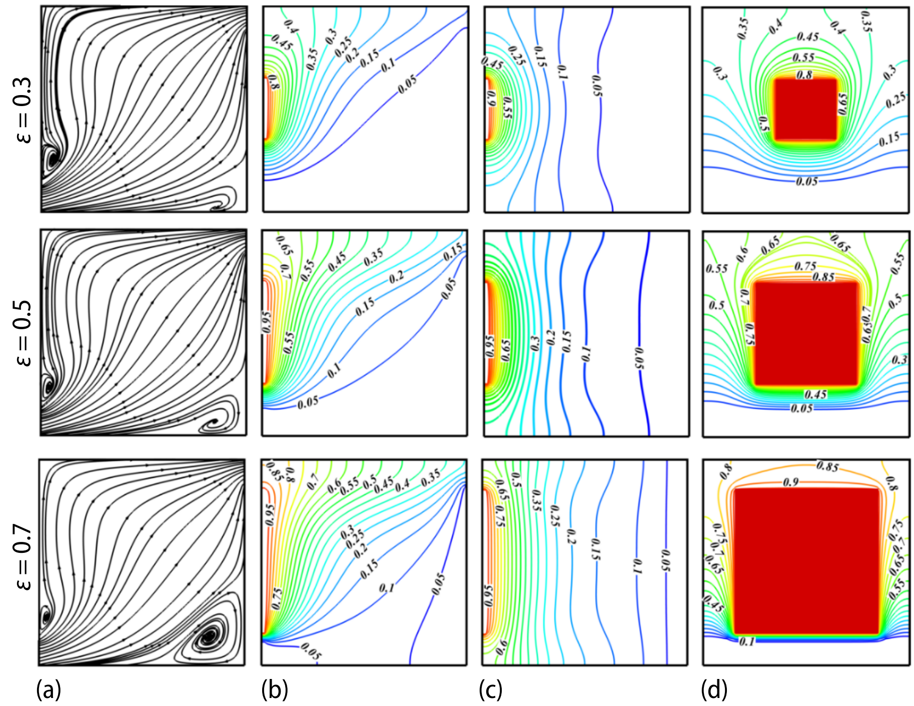

Figure 7. Streamlines (a) at the middle plane $Z = 0.5$ and isotherms at the planes, (b) $Z = 0.5$, (c) $Y = 0.5$, and (d) $X = 0.025$ for Ri = 1, Re = 100 and different ε values

creasing the heating section ε, the size and intensity of the first re-circulation are slightly reduced, while the second one is increased.

The horizontal velocity profiles $U(Y)$, fig. 8(a) near the vicinity of the left wall $(X = 0.25)$ increases until reaching a maximum value between the inlet-opening and the heated surface. It can be seen that the increase of the heating surface ε leads to the decrease of the horizontal velocity. In fact, at this location, the small convective cell appears and it increases in size when the section dimension ε decreases. This is due to the combined effects of the inertia force and thermal buoyancy in the vertical direction, then the $U(y)$ decreases and keep the same trend in the middle of the heated section reaching a minimum value (incoming cold flow) then increases slightly by increasing ε in the upper part until zero. On the other hand, the same ε effect is observed for $U(Y)$, fig. 8(b) and the W component, fig. 8(c). It should be noted that the W velocity profile along the Z-direction is different to zero value which means the movement is always 3-D.

The 3-D distribution of temperature fields is illustrated in fig. 9, the isotherms structure is more clustered near the heated surface for the small cross-section $\varepsilon = 0.3$ attesting of a better heat exchange in the cavity and it becomes stratified and less concentrated when the cross-sections increase in size. This behavior is attributed to the fact that mixed convection is established rapidly for the small heated surface in which, the heat exchange between the active surface and the incoming flow improve favorably the balance between inertia and buoyancy forces. The increase of the heating sections gives a clear indication of the conjugate effect of conduction and mixed convection flow in the cavity.

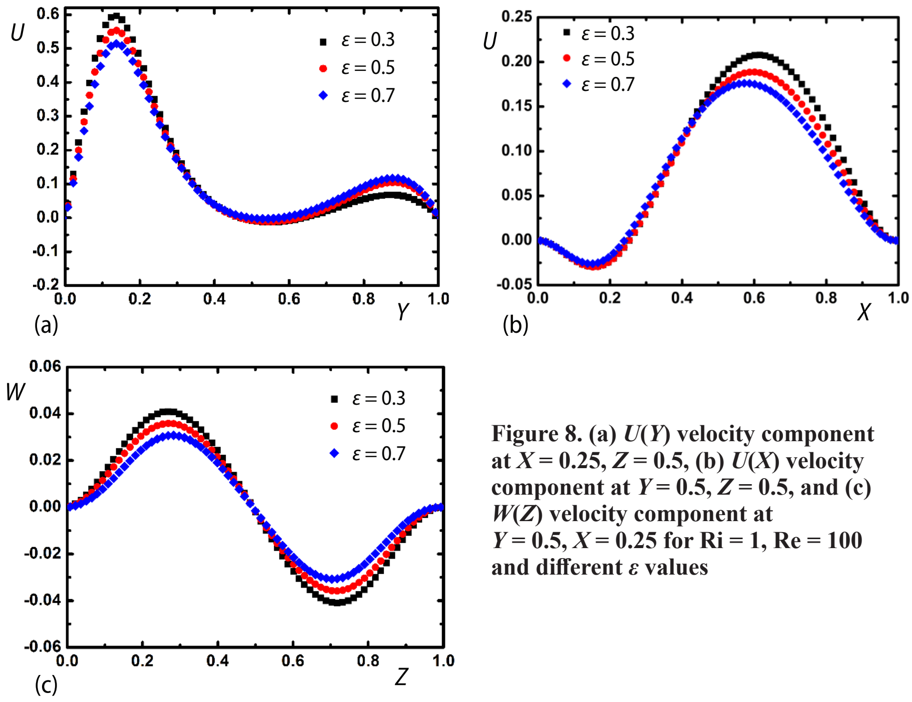

Figure 8. (a) $U(Y)$ velocity component at $X = 0.25$, $Z = 0.5$, (b) $U(X)$ velocity component at $Y = 0.5$, $Z = 0.5$, and (c) $W(Z)$ velocity component at $Y = 0.5$, $X = 0.25$ for Ri = 1, Re = 100 and different ε values

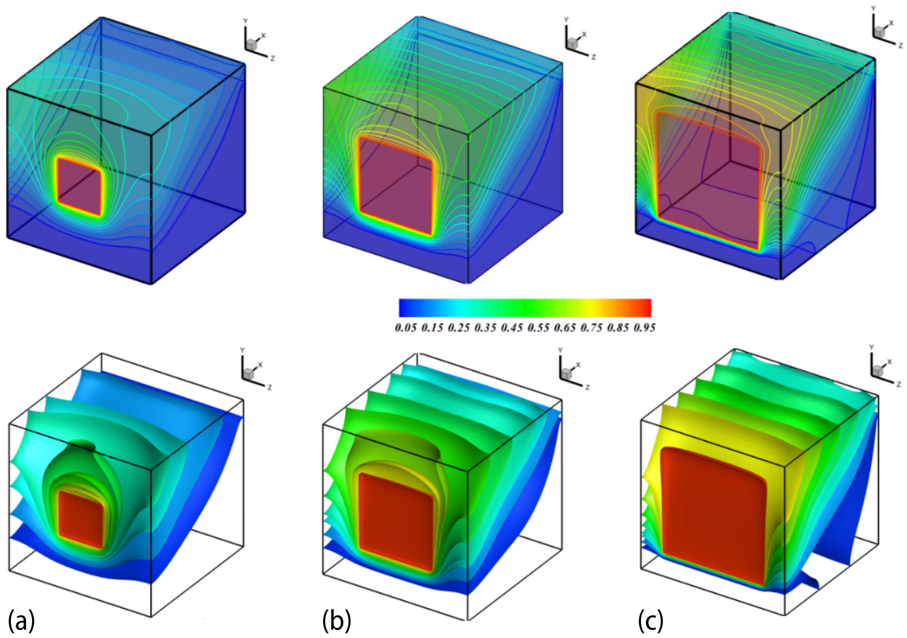

Figure 9. Temperature contour (top) and temperature iso-surfaces (bottom) for (a) $\varepsilon = 0.3$, (b) $\varepsilon = 0.5$, (c) $\varepsilon = 0.7$ and Ri = 1, Re = 100

Heat transfer

In order to analyze the heat transfer performance for the studied configuration, we present the variations of the global average Nusselt numbers calculated on the heating sections as a function of Ri and ε for different Reynolds values fig. 10

We can notice that the Nusselt number increases with increasing Richardson and Reynolds numbers for all the considered heating section dimension ε. On the other hand, for the low Reynolds number (Re = 10) a slightly significant difference of the Nusselt number by increasing Richardson number since the interaction between inertia and buoyancy effects are still weak, which leads to a slow development of the mixed convection, resulting in a heat transfer dominated by conduction heat transfer at the vicinity of the heating sections. The decrease of the portion dimension ε enhances significantly the cooling rate on the heated section. This is due to fast exchange between the external incoming flow and the heating zone, which precipitates the establishment of the mixed convection mode.

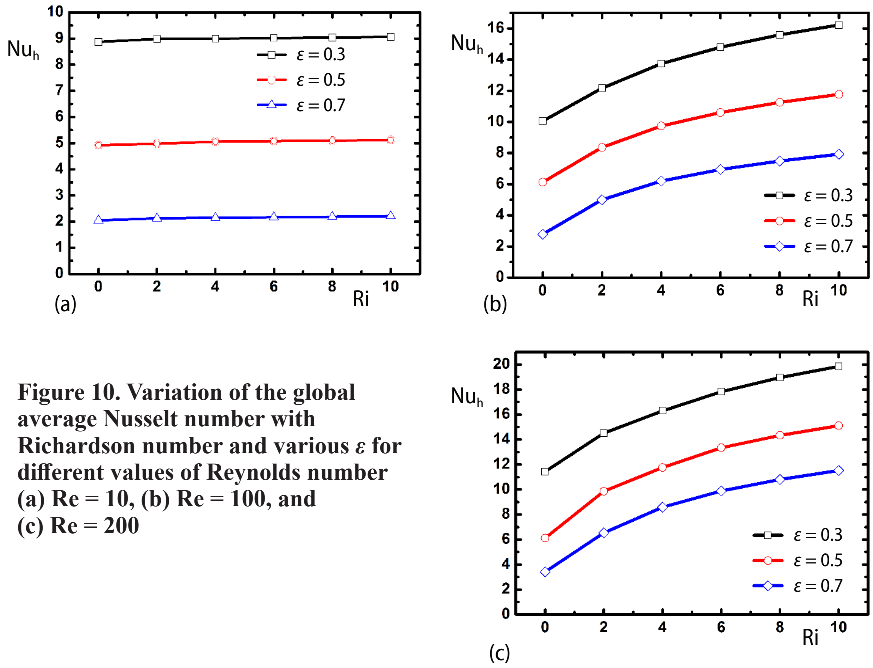

Figure 10. Variation of the global average Nusselt number with Richardson number and various ε for different values of Reynolds number (a) Re = 10, (b) Re = 100, and (c) Re = 200

Conclusion

A computational study was performed to investigate the mixed convection in a 3-D a ventilated cavity discretely heated from the side using the finite volume model for different governing parameters (Reynolds and Richardson numbers and heating section dimensions). The main conclusions of the present study can be summarized as follows.

- The flow structures and temperature distribution are considerably affected by the interaction between the inertia and the buoyancy forces.
- The mixed convection is installed rapidly in the case of the small heating surfaces.
- For the low Reynolds number (Re = 10) and for all considered heating surface dimension ε, the heat transfer process is carried out by conduction and the Nusselt number values are almost unchanged by increasing Richardson number.

- For fixed heating section dimension ε, the global Nusselt number increases by increasing Richardson and Reynolds numbers.
- For fixed Richardson and Reynolds numbers, the average Nusselt number increases with decreasing heating section dimensions ε.

Nomenclature

B – relative height of the openings, ($= h/L$)
c – lenght of a side of isothermal hot portion
g – acceleration due to gravity, [ms^{-2}]
Gr – Grashof number, [–]
h – height of the openings, [m]
H – height of the cavity, [m]
L – length of the cavity, [m]
Nu – Nusselt number, [–]
P – dimensionless pressure, [–]
Pr – Prandtl number, [–]
Re – Reynolds number, [–]
Ri – Richardson number, [–]
T – ambient temperature, [°C]
u, v, w – dimensional velocities, [ms^{-1}]
U, V, W – dimensionless velocity components, [–]
x, y, z – dimensional co-ordinates, [m]
X, Y, Z – dimensionless cartesian co-ordinates, [–]

Greek symbols

α – thermal diffusivity, [m^{2}s^{-1}]
ε – heating sections dimension, ($= c/L$)
θ – non-dimensional temperature, [–]
β – volumetric thermal expansion coefficient, [K^{-1}]
ν – kinematic viscosity, [m^{2}s^{-1}]
ρ – density, [kgm^{-3}]

Subscripts

c – cold
h – hot
i, j, k – node position
in – inlet

References

[1] Papanicolaou, E., Jaluria, Y., Mixed Convection from a Localized Heat Source in a Cavity with Conducting Walls: A Numerical Study, *Numerical Heat Transfer, Part A Applications*, *23* (1993), 4, pp. 463-484
[2] Yucel, C., *et al.*, Mixed Convection Heat Transfer in Open Ended Inclined Channels with Discrete Isothermal Heating, *Numerical Heat Transfer, Part A*, *24* (1993), 1, pp. 109-126
[3] Shuja, S. Z., *et al.*, Mixed Convection in a Square Cavity due to Heat Generating Rectangular Body, *International Journal of Numerical Methods for Heat & Fluid Flow*, *10* (2000), 8, pp. 824-841
[4] Manca, O., *et al.*, Effect of Heated Wall Position on Mixed Convection in a Channel with an Open Cavity, *Numer. Heat Transfer, Part A, 43* (2003), 3, pp. 259-282
[5] Bahlaoui, A., *et al.,* Coupling between Mixed Convection and Radiation in an Inclined Channel Locally Heated, *J. Mech. Eng., 55* (2004), Jan., pp. 45-57
[6] Bhoite, M. T., *et al.,* Mixed Convection in a Shallow Enclosure with a Series of Heat Generating Components, *Int. J. Thermal Sciences*, *44* (2005), 2, pp. 121-135
[7] Saha, S., *et al.,* Combined Free and Forced Convection Inside a Two-Dimensional Multiple Ventilated Rectangular Enclosure, *ARPN Journal of Engineering and Applied Sciences, 1* (2006), 3, pp. 23-35
[8] Manca, O., *et al.,* Experimental Investigation of Mixed Convection in a Channel with an Open Cavity, *Experimental Heat Transfer*, *19* (2006), 1, pp. 53-68
[9] Raji, A., *et al.,* Numerical Study of Natural Convection Dominated Heat Transfer in a Ventilated Cavity: Case of Forced Flow Playing Simultaneous Assisting and Opposing Roles, *International Journal of Heat and Fluid Flow*, *29* (2008), 4, pp. 1174-1181
[10] Bahlaoui, A., *et al.,* Mixed Convection Cooling Combined with Surface Radiation in a Partitioned Rectangular Cavity, *Energy Conversion and Management*, *50* (2009), 3, pp. 626-635
[11] Bahlaoui, A., *et al.,* Height Partition Effect on Combined Mixed Convection and Surface Radiation in a Vented Rectangular Cavity, *Journal of Applied Fluid Mechanics*, *4* (2011), 1, pp. 89-96
[12] Gupta, S. K., *et al.,* Investigation of Mixed Convection in a Ventilated Cavity in the Presence of a Heat Conducting Circular Cylinder, *Numer. Heat Transfer, Part A, 67* (2015), 1, pp. 52-74
[13] Papanicolaou, E., Jaluria, Y., Mixed Convection from an Isolated Heat Source in a Rectangular Enclosure, *Numerical Heat Transfer*, *18* (1991), 4, pp. 427-461
[14] Hsu, T. H., *et al.*, Mixed Convection in a Partially Divided Rectangular Enclosure, *Numerical Heat Transfer, Part A Applications, 31* (1997), 6, pp. 655-683

[15] Raji, A., Hasnaoui, M., Mixed Convection Heat Transfer in a Rectangular Cavity Ventilated and Heated From the Side, *Numerical Heat Transfer, Part A Applications, 33* (1998), 5, pp. 533-548
[16] Raji, A., Hasnaoui, M., Corrélations en convection mixte dans des cavités ventilées, *Revue générale de thermique, 37* (1998), 10, pp. 874-884
[17] Omri, A., Ben Nasrallah, S., Control Volume Finite Element Numerical Simulation of Mixed Convection in an Air-Cooled Cavity, *Numer. Heat Transfer, Part A, 36* (1999), 6, pp. 615-637
[18] Raji, A., Hasnaoui, M., Mixed Convection Heat Transfer in Ventilated Cavities with Opposing and Assisting Flows, *Engineering Computations*, *17* (2000), 5, pp. 556-572
[19] Raji, A., Hasnaoui, M., Combined Mixed Convection and Radiation in Ventilated Cavities, *Eng. Comput: Int. J. Computer-Aided Eng. Software*, *18* (2001), 7, pp. 922-949
[20] Singh, S., Sharif, M. A. R., Mixed Convective Cooling of a Rectangular Cavity with Inlet and Exit Openings on Differentially Heated Side Walls, *Numerical Heat Transfer: Part A: Applications, 44* (2003), 3, pp. 233-253
[21] Saha, *et al.*, Mixed Convection in an Enclosure with Different Inlet and Exit Configurations, *Journal of Applied Fluid Mechanics*, *1* (2008), 1, pp. 78-93
[22] Rahman, *et al.*, Effect of the Presence of a Heat Conducting Horizontal Square Block on Mixed Convection Inside a Vented Square Cavity, *Nonlinear Analysis: Modelling and Control*, *14* (2009), 4, pp. 531-548
[23] Rahman, M. M., *et al.* Effects of Reynolds and Prandtl Number on Mixed Convection in a Ventilated Cavity with a Heat-Generating Solid Circular Block, *Applied Mathematical Modelling*, *36* (2012), 5, pp. 2056-2066
[24] Frederick, R. L., Quiroz, F., On the Transition from Conduction to Convection Regime in a Cubical Enclosure with a Partially Heated Wall, *International Journal of Heat and Mass Transfer*, *44* (2001), 9, pp. 1699-1709
[25] Ben-Cheikh, N., *et al.*, Three-Dimensional Study of Heat and Fluid Flow of Air and Dielectric Liquids Filling Containers Partially Heated from Below and Entirely Cooled from Above, *International Communications in Heat and Mass Transfer*, *37* (2010), 5, pp. 449-456
[26] Stiriba, Y., *et al.*, A Numerical Study of Three-Dimensional Laminar Mixed Convection Past an Open Cavity, *International Journal of Heat and Mass Transfer*, *53* (2010), 21, pp. 4797-4808
[27] Moraga, N. O., Lopez, S. E., Numerical Simulation of Three-Dimensional Mixed Convection in an Air-Cooled Cavity, *Numerical Heat Transfer, Part A: Applications*, *45* (2004), 8, pp. 811-824
[28] Tariq, J., *et al.*, Mixed Convection Boundary-Layer Flow of a Viscoelastic Fluid Due to Horizontal Elliptic Cylinder with Constant Heat Flux, *Thermal Science, 22* (2018), 1B, pp, 567-575
[29] Doghmi, H., *et al.*, Effect of the Inlet Opening on Mixed Convection Inside a Three-Dimensional Ventilated Cavity, *Thermal Science, 22* (2018), 6A, pp. 2413-2424
[30] Patankar, S. V., *Numerical Heat Transfer and Fluid Flow,* McGraw-Hill, New York, USA, 1980

Paper submitted: April 10, 2018
Paper revised: June 27, 2018
Paper accepted: June 28, 2018